Protein Science (1994), *3*:1493-1503. Cambridge University Press. Printed in the USA.

Computer modeling of substrate binding to lipases from *Rhizomucor miehei*, *Humicola lanuginosa*, and *Candida rugosa*

MARTIN NORIN,[1] FREDRIK HAEFFNER,[2] ADNANE ACHOUR,[1]
TORBJÖRN NORIN,[2] AND KARL HULT[1]

[1] Department of Biochemistry and Biotechnology and [2] Department of Chemistry, Organic Chemistry, Royal Institute of Technology, S-100 44 Stockholm, Sweden

(RECEIVED May 2, 1994; ACCEPTED June 28, 1994)

Abstract

The substrate-binding sites of the triacyl glyceride lipases from *Rhizomucor miehei*, *Humicola lanuginosa*, and *Candida rugosa* were studied by means of computer modeling methods. The space around the active site was mapped by different probes. These calculations suggested 2 separate regions within the binding site. One region showed high affinity for aliphatic groups, whereas the other region was hydrophilic. The aliphatic site should be a binding cavity for fatty acid chains. Water molecules are required for the hydrolysis of the acyl enzyme, but are probably not readily accessible in the hydrophobic interface, in which lipases are acting. Therefore, the hydrophilic site should be important for the hydrolytic activity of the enzyme.

Lipases from *R. miehei* and *H. lanuginosa* are excellent catalysts for enantioselective resolutions of many secondary alcohols. We used molecular mechanics and dynamics calculations of enzyme-substrate transition-state complexes, which provided information about molecular interactions important for the enantioselectivities of these reactions.

Keywords: calculation; enantioselectivity; free energy; water

Lipases are enzymes that hydrolyze triacyl glycerides, thus liberating fatty acids. These enzymes are commercially important as constituents of washing detergents and as catalysts in industrial transesterifications of fats. The objective of this study was to increase our understanding of the enzyme-substrate interactions of the 2 homologous lipases from *Rhizomucor miehei* and *Humicola lanuginosa* by means of molecular modeling techniques. Lipases are able to catalyze a number of mutually related nucleophilic substitutions and are widely used in preparative biotransformations of organic molecules. Lipase from *R. miehei* shows high activity in various organic solvents (Sonnet & Moore, 1988) and is therefore a useful biocatalyst in bioorganic synthesis. The molecular structure of the *R. miehei* lipase has been thoroughly investigated by means of X-ray crystallography (U. Derewenda et al., 1992; Z.S. Derewenda et al., 1992). However, our knowledge of the molecular details of its substrate binding is poor. At the time of this writing, only 1 detailed structure of a lipase-inhibitor complex (Brzozowski et al., 1991; U. Derewenda et al., 1992) is currently available (Kinemage 1). In addition, we investigated the binding regions in the active site of the lipase from *Candida rugosa*. This lipase is structurally different from the 2 fungal lipases, although the α/β-hydrolase fold (Ollis et al., 1992) of all 3 lipases studied is conserved. Recently, it has been shown for the *C. rugosa* lipase that a tunnel, which is unique among lipases studied to this date, is involved in the binding of the scissile fatty acid chain (Grochulski et al., 1994a). The modeled binding regions of this lipase in this work are compared with those of the 2 fungal lipases.

The active sites of the lipases were mapped by means of a method called GRID (Goodford, 1985). This method has recently been used to design inhibitors of influenza virus replication (von Itzstein et al., 1993) and to elucidate the catalytic mechanism of phospholipase C (Byberg et al., 1992). A cubic lattice is placed in the space to be studied. At each grid point of the lattice, the interactions of a probe with the target molecule are calculated by an energy function. The resulting potential maps are analyzed by means of a molecular graphics program to visualize interesting binding regions.

The catalytic mechanisms of lipases are most probably similar to those of serine proteases. A catalytic triad, Ser-His-Asp/Glu, is involved in an acid-base-catalyzed cleavage of ester bonds. Also important is the stabilization of a charged oxygen

Reprint requests to: Karl Hult, Department of Biochemistry and Biotechnology, Royal Institute of Technology, S-100 44 Stockholm, Sweden; e-mail: kalle@biochem.kth.se.

atom in the transition state of the hydrolytic reaction. The charged oxygen atom is believed to be stabilized by hydrogen bonds in an "oxyanion hole." The stereochemistry of the oxyanion hole of the *R. miehei* lipase is not clear (Derewenda & Sharp, 1993). Lipases are activated at hydrophobic surfaces (Sarda & Desnuelle, 1958) through movements of 1 or a few surface loops that bury the active site in the inactive conformation (Winkler et al., 1990; Brzozowski et al., 1991; U. Derewenda et al., 1992, 1994; van Tilbeurgh et al., 1992, 1993; Grochulski et al., 1993). The lipase from *R. miehei* has 1 helix, covering the active site like a lid, which opens during activation (Brady et al., 1990; Brzozowski et al., 1991; U. Derewenda et al., 1992; Z.S. Derewenda et al., 1992). It has been proposed, on the basis of X-ray crystallographic studies, that the oxyanion hole of lipases from *R. miehei* and human pancreas can exist only in the open active conformation (Brzozowski et al., 1991; Derewenda & Sharp, 1993; van Tilbeurgh et al., 1993). In contrast, the oxyanion hole appears to be preformed in the closed inactive form of the *C. rugosa* lipase (Grochulski et al., 1994b). We used molecular dynamics simulations of transition-state complexes to study the hydrogen bonding networks of the catalytic machineries of the *R. miehei* and the *H. lanuginosa* lipases. From the simulation result, we propose a somewhat different stereochemistry of the oxyanion hole than previously suggested (Brzozowski et al., 1991; Derewenda & Sharp, 1993).

The enantioselectivities of reactions catalyzed by the *R. miehei* lipase and other closely related lipases from filamentous fungi make these reactions suitable for resolving chiral secondary alcohols (Sonnet, 1987; Sonnet & Baillargeon, 1987; Sonnet & Moore, 1988; Janssen et al., 1991). We combined energy minimization and molecular dynamics simulations for investigating the stereospecific properties of these lipases. Recently, we applied this method for calculating enantioselectivities of reactions catalyzed by chymotrypsin (Norin et al., 1993). We have, in the work presented here, investigated 2 chiral substrates, which are shown in Figure 1. GRID calculations and X-ray crystal structures of lipase-inhibitor complexes were used as models for docking the substrates with the enzyme.

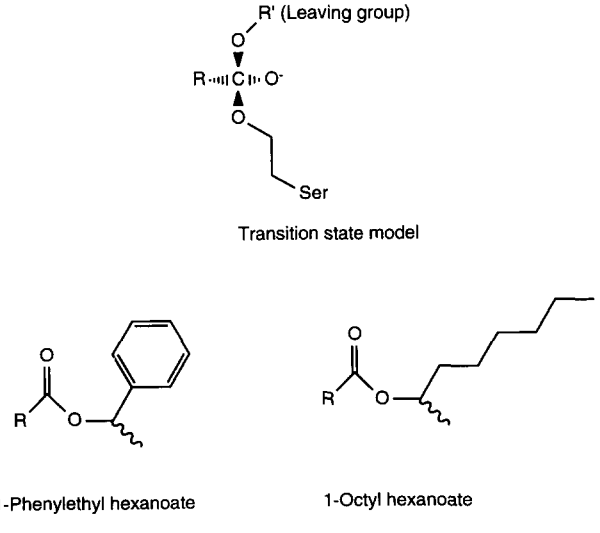

Fig. 1. The transition-state model used in the calculations and the structures of the chiral substrates investigated.

Results

Assumed enzymatic reaction mechanism

Lipases catalyze the hydrolysis and the interesterifications of ester groups. The reaction mechanism is assumed to be analogous to that of serine proteases. Crucial in the reaction mechanism is a catalytic triad consisting of the amino acid residues Asp, His, and Ser (Fig. 2). A charged oxygen atom in the transition state is stabilized in the "oxyanion hole." The substrates consist of an acyl moiety and a leaving alcohol group. The substrate forms a Michaelis–Menten complex in a substrate-binding pocket. The reactive carbonyl carbon atom is then attacked by the hydroxyl group of the active-site serine residue to form a tetrahedral intermediate (Figs. 1, 2). This intermediate is considered to be close to the transition state of the reaction. The hydrogen atom of the hydroxyl group of the serine is transferred to the histidine of the catalytic triad during the attack. The carbonyl oxygen atom forms a negatively charged single-bonded oxyanion. The tetrahedral intermediate subsequently breaks down to form an acyl enzyme. The protonated imidazole ring donates a proton to the leaving alcohol group. The acyl enzyme is then hydrolyzed by water or cleaved by a competing nucleophile through an analogous pathway in which 1 proton is transferred from the nucleophile through the imidazole group to the active-site serine residue.

Binding sites calculated by GRID

The natural substrates for lipases are triacyl glycerides, which partly consist of long-chain aliphatic fatty acid residues. The result of the GRID calculation of the *R. miehei* lipase using an aliphatic group as the probe is shown in Figure 3A. The most favorable region for the aliphatic probe was the hydrophobic groove in the active site. In the crystal structure of the lipase, this site is partly occupied by a short aliphatic chain of the inhibitor, which mimics the acyl group of the substrate.

In the crystal structure of the open form of *H. lanuginosa* lipase, the transition-state inhibitor contains a long-chain aliphatic group of 12 carbon atoms. We repeated the GRID calculations on the *H. lanuginosa* lipase and observed very similar results to

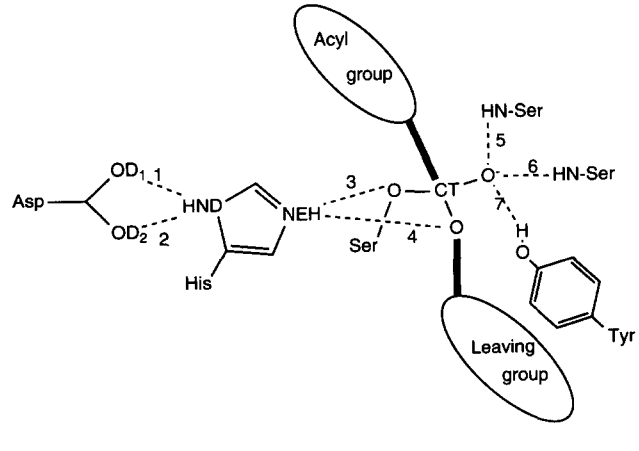

Fig. 2. Schematic picture of the transition-state model in the reaction center of the lipases. Important distances are marked with dashed lines.

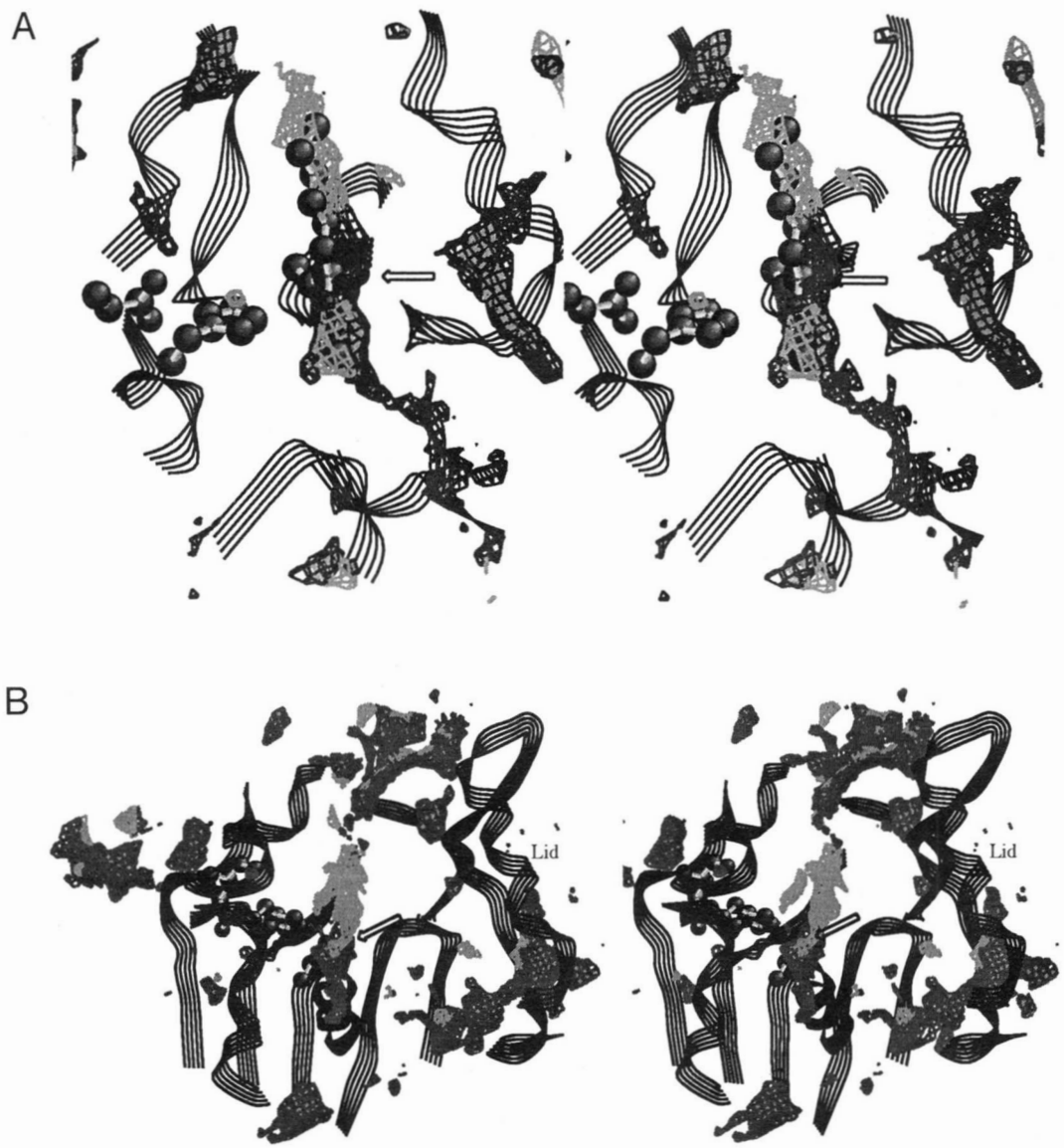

Fig. 3. Contour maps in the active sites calculated by GRID. Contours at −3.0 kcal/mol for a methyl probe are shown in gray. Contours at −6.5 kcal/mol for a water probe are shown in black. Neighboring parts of the backbone of the enzyme are indicated by ribbons. The arrows indicate the reaction center of the enzymes. The catalytic triads are indicated using ball and stick models. **A:** The *R. miehei* lipase. A hexyl phosphonate transition-state inhibitor in the 5TGL structure is indicated using ball and stick models. The helix to the right of the catalytic center is the lid. **B:** The *C. rugosa* lipase. The position of the lid is labeled.

those of the *R. miehei* lipase. The aliphatic site was somewhat longer and spanned over the 12 carbon atoms of the aliphatic chain of the inhibitor.

No strong additional binding sites for aliphatic carbon or carbonyl oxygen atoms could be found in the active sites of any of the lipases. Thus, we could not find any specific binding sites for a leaving diacyl glyceride group.

Lipases require water to hydrolyze the acyl enzyme. However, the access to water in the hydrophobic interface around the active site may be limited. The low water activity may be compensated by a trap for water molecules in the active site. Such a trap has been briefly mentioned in a report of an X-ray crystallography study of the *Geotrichum candidum* lipase (Schrag & Cygler, 1993). We investigated the binding of water molecules to the active site of the *R. miehei* lipase. The GRID program was used and the result is shown in Figure 3A. A favorable binding site for water was found at the bottom of the groove of the active site. This site was positioned opposite to the aliphatic site described above. The water site spanned about 14 Å from a hydrophilic part of the protein surface into the active site and ended up at the reaction center of the enzyme. GRID calculations of the *H. lanuginosa* lipase again gave similar results. Calculations of water-binding sites in the modeled acyl enzymes showed that the hydrophilic site may accommodate a water molecule in a position that is favorable for an in-plane nucleophilic attack on the carbonyl carbon atom of the acyl group (Fig. 4).

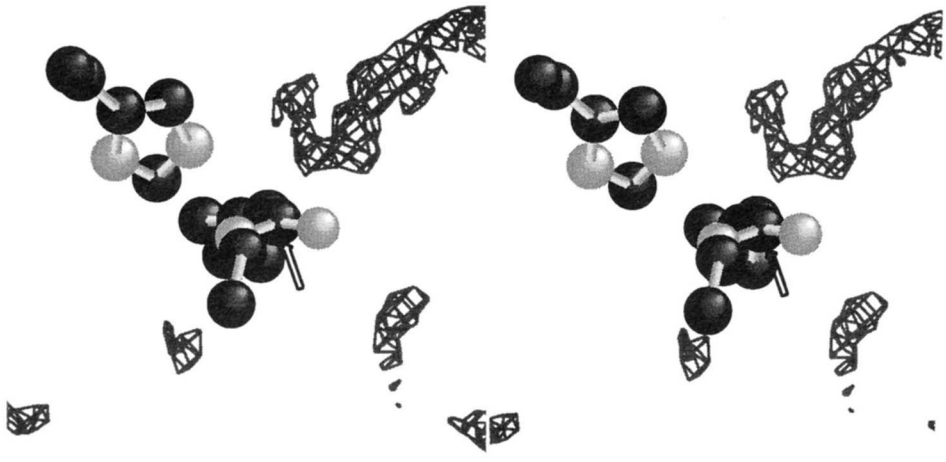

Fig. 4. Contours of a water probe at −6.5 kcal/mol around the acyl enzyme of the *R. miehei* lipase. The Ser-O-CO-R acyl group is to the right of His-257. Carbon atoms are shown in black. The reactive carbonyl carbon atom is indicated with an arrow. Non-carbon atoms (oxygen and nitrogen atoms) are shown in gray.

Furthermore, in this position, the water molecule may donate 1 hydrogen bond to the imidazole of the catalytic triad, which is proposed to act as a base in the catalytic reaction.

Comparison with C. rugosa lipase

GRID calculations of lipase from *C. rugosa* were performed using water and aliphatic probes (Fig. 3B). In the lipase from *C. rugosa*, there is long tunnel extending from the active Ser-209 into the center of the protein (Grochulski et al., 1994b). The end of the tunnel is blocked by the C-terminal residues. GRID highlighted an aliphatic binding site in this tunnel. During the preparation of this paper, an X-ray crystallography study of the *C. rugosa* lipase complexed with inhibitors was published. This study revealed that the tunnel is involved in the binding of the scissile fatty acid chain. A structural alignment (Kinemage 2) of the α/β-hydrolase folds (Ollis et al., 1992) of the *R. miehei* and the *C. rugosa* lipases reveals that the inhibitor of the *R. miehei* lipase is remarkably well oriented in the tunnel (Grochulski et al., 1994b). The GRID calculations indicated favorable affinities for water at the reaction center of the *C. rugosa* lipase and between the lid and the core of the enzyme.

Calculations of chiral substrate–lipase transition-state complexes

Lipases from *R. miehei* and *H. lanuginosa* have proved to be excellent catalysts for enantiomeric resolutions of many secondary alcohols (Sonnet, 1987; Sonnet & Baillargeon, 1987; Sonnet & Moore, 1988; Macfarlane et al., 1990; Janssen et al., 1991). Transition-state models of 1-phenylethyl and 2-octyl hexanoate esters (Fig. 1) were modeled in the active sites of the lipases. The same orientations for the large groups, phenyl and hexyl, of both enantiomers were used as starting structures for the calculations, i.e., only the positions of the methyl group attached to the chiral carbon atom of the substrate differed. Energy minima of the substrate–enzyme complexes were found by using molecular dynamics simulations and energy minimizations. The lowest energy minimum of each enzyme–substrate complex will be abbreviated as follows. The (*R*,*S*)-1-phenylethyl hexanoate and the (*R*,*S*)-2-octyl hexanoate complexes with the *R. miehei* lipase are abbreviated as R-PHERM, S-PHERM, R-OCTRM, and S-OCTRM for each enantiomer, respectively. The energy minima of the (*R*,*S*)-1-phenylethyl hexanoate complexes with the *H. lanuginosa* lipase are abbreviated as R-PHEHL and S-PHEHL. The calculated binding orientations of the substrates of the R-PHERM, R-OCTRM, and R-PHEHL structures were similar (Fig. 5A). The binding modes of the substrates of the fast-reacting *R*-enantiomers did not differ much from the starting conformation. The phenyl and hexyl groups of the leaving alcohols pointed perpendicularly to the bottom of the active site. The methyl groups occupied a small cavity in the active site. In the *R. miehei* lipase, this cavity is formed by the backbone atoms of Gly-266 and the side-chain atoms of Tyr-28, His-143, His-257 (involved in the catalytic triad), and Leu-258 (Fig. 6). The slow-reacting *S*-enantiomers bonded differently from the preferred *R*-enantiomers. The methyl groups of the *S*-enantiomers preferred to occupy positions similar to those of the phenyl and hexyl groups of the *R*-enantiomers (Fig. 5B). The phenyl and hexyl groups were oriented along the ditchlike cavity of the active site. The structures of R-PHERM and S-PHERM are shown in Kinemage 3. The potential energies of the lowest energy minima of the transition states of each pair of substrates are compared in Table 1. The energies of the slow-reacting *S*-enantiomers were higher, indicating that these structures were more strained than those of the *R*-enantiomers.

Free energy calculations

The differences in free energies between the enantiomers of the transition-state models were calculated by means of molecular dynamics simulations in which the substrates were slowly perturbed between the 2 enantiomeric states. The total simulation times for converting the models from one enantiomer to the other were 120 or 240 ps using a stepsize, $\Delta\lambda$, of 0.05 or 0.0025, respectively. The simulations were first performed in a forward direction (λ going from 0 to 1). After equilibration during 10 ps, the simulations were reversed (λ going from 1 to 0). The free energy barriers in the transition pathway were between 2 and 6 kcal/mol. Large hystereses of the free energy values in the perturbation pathway prevented us from estimating the free energy differences between the enantiomeric states. An analysis of the trajectories showed that the errors were due to both problems with fluctuations and the fact that the free energy derivatives

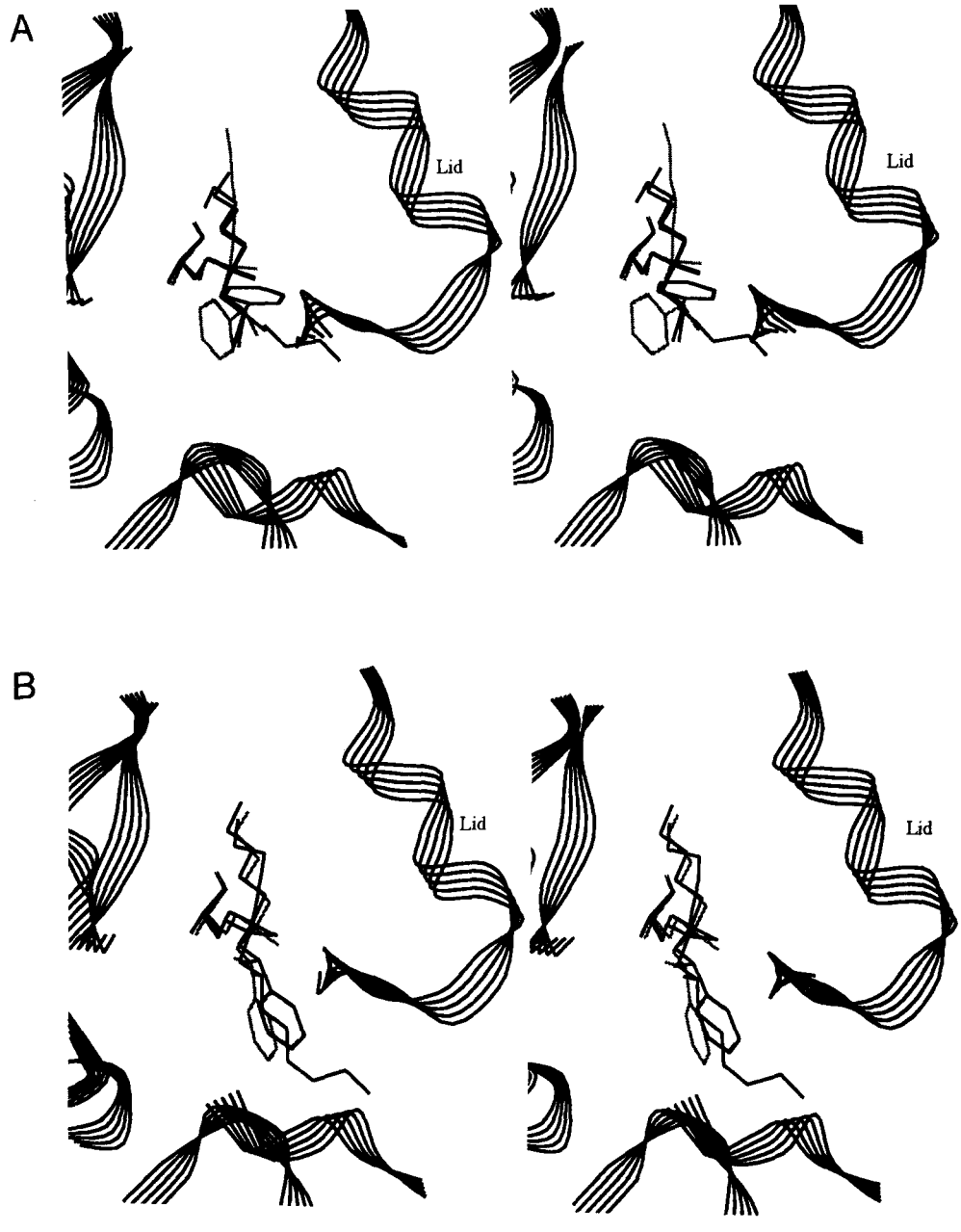

Fig. 5. The structures at the energy minima of the transition-state models. The backbone of the enzyme is indicated by ribbons. The lid is labeled. **A:** The fast-reacting *R*-enantiomers. R-PHERM and R-OCTRM are in black and R-PHEHL is gray. **B:** The slow-reacting *S*-enantiomers. S-PHERM and S-OCTRM are shown in black and S-PHEHL in gray.

at each step did not converge. The binding orientations of the substrates were similar to those calculated as presented in the preceding paragraphs.

Hydrogen bonding in the catalytic center

The hydrogen bonds existing at the energy minimum of each calculated enzyme–substrate complex were analyzed in both lipases. The atomic distances between atoms involved in important hydrogen bonds are shown in Table 2. The hydrogen bonds of the aspartate carboxyl group in the catalytic triad were very stable throughout all molecular dynamics simulations. Both oxygen atoms of the carboxyl group were bridgeheads of hydrogen bonds. One oxygen atom hydrogen bonded to an amide backbone group and the other to the side chain of a tyrosine residue (Fig. 7). In addition, one or both of the carboxyl oxygen atoms hydrogen bonded to the histidine side chain of the catalytic triad. The protonated histidine group in the triad formed a hydrogen bond to the oxygen atom of the leaving alcohol group of the substrate in all structures. In all energy minima, except for the R-PHEHL structure, the distances between the Hϵ2 atom of the histidine and the hydroxyl oxygen atom of the serine were some-

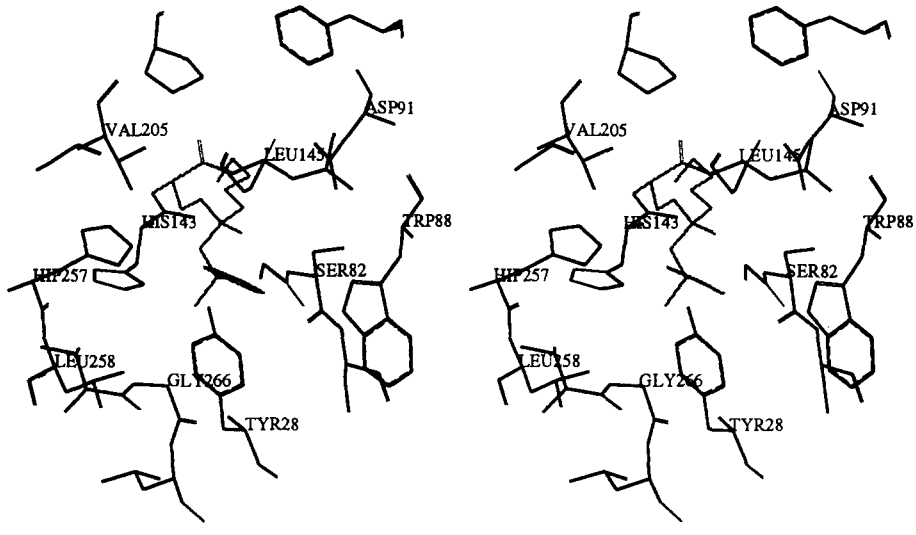

Fig. 6. The stereochemistry of the active site of the *R. miehei* lipase is shown in black using the R-PHERM structure. The serine-substrate transition-state complex is drawn in gray.

what longer than what is expected for fully developed hydrogen bonds.

The oxyanion in the tetrahedral intermediates formed 2 hydrogen bonds to amide groups of the protein backbone. The amide groups belonged to Leu-145 and Ser-82 residues of the *R. miehei* lipase (Fig. 7) and the corresponding amino acids Leu-147 and Ser-83 of the *H. lanuginosa* lipase. In the R-PHEHL structure, the oxyanion formed an additional hydrogen bond to the side chain of Ser-83. In the *R. miehei* structures, the side chain of this serine residue was hydrogen bonded to the side chain of Asp-91 in the lid (Fig. 7). In the *H. lanuginosa* structures, the side chain of Ser-83 hydrogen bonded to Asn-93.

Although the free energy perturbation calculations did not provide sufficient precision in the energy estimations, some interesting structural features were seen during the simulations. Small rearrangements of the reaction center of the *R. miehei* lipase caused the oxyanion to form an additional hydrogen bond to the hydroxyl group of Tyr-28. To further investigate the stereochemistry of the oxyanion hole, we performed a molecular dynamics simulation at 300 K starting with the R-PHERM structure. In Figure 8 the atomic distances between the oxyanion and candidates for its hydrogen bonding partners are shown versus the simulation time. The shortest and most stable hydrogen bond was that connecting the oxyanion with the amide group of Ser-82. The hydrogen bond to the amide of Leu-145 was slightly longer and showed larger fluctuations. The distance between the oxyanion and the hydroxyl proton of Tyr-28 was longer than the latter ones and fluctuated around 3.2 Å. This distance is somewhat longer that what is expected for a fully developed hydrogen bond, but still short enough to provide for favorable interactions between the oxyanion and the hydroxyl group. The side chain of Ser-82 formed a stable hydrogen bond with the side chain of Asp-91 during the simulation.

Table 1. *Differences in potential energies ($\Delta\Delta V$) between the transition-state complexes of the R- and S-enantiomers of the substrates and corresponding experimental values of differences of the activation energies of the enzymatic reactions ($\Delta\Delta G$)*

Structures	$\Delta\Delta V$[a] (kcal/mol)	$\Delta\Delta G$[b] (kcal/mol)
R- and S-PHERM	−2.4	−2.2
R- and S-OCTRM	−4.4	<−2.4
R- and S-PHEHL	−0.5	−1.9

[a] The $\Delta\Delta V$ values were calculated as the differences of the total potential energies between the transition-state complexes of the enantiomers ($V_R - V_S$). Because the energies of the ground-state unliganded species of the enantiomers are equal, it is sufficient to calculate the difference in energy of the transition states.

[b] Experimental values of *R,S*-PHERM and *R,S*-PHEHL were calculated from unpublished kinetic studies by Fredrik Haeffner. The value of *R,S*-OCTRM was estimated from kinetic studies by Sonnet (1987) and Janssen et al. (1991). The $\Delta\Delta G$ values were calculated as $\Delta\Delta G = -RT * \ln[(k_{cat}/K_m)_R/(k_{cat}/K_m)_S]$.

Discussion

The GRID calculations were used to identify aliphatic and hydrophilic binding sites. Regions that were favorable to a methyl probe but not to a water probe were regarded as hydrophobic

Table 2. *Distances (Å) between hydrogen bonding partners in the catalytic center of the calculated transition-state complexes*

Structure	Distances as shown in Figure 2						
	1	2	3	4	5	6	7
R-PHERM	1.7	2.4	3.0	1.9	2.0	1.8	3.3
S-PHERM	1.7	2.4	3.1	1.9	2.3	1.8	3.6
R-OCTRM	1.7	2.4	2.9	1.8	2.0	1.8	3.2
S-OCTRM	1.7	2.4	2.8	1.8	2.0	1.8	3.6
R-PHEHL	1.7	2.5	2.6	1.8	2.1	1.8	3.8
S-PHEHL	1.7	2.5	2.9	1.8	2.8	1.8	3.4

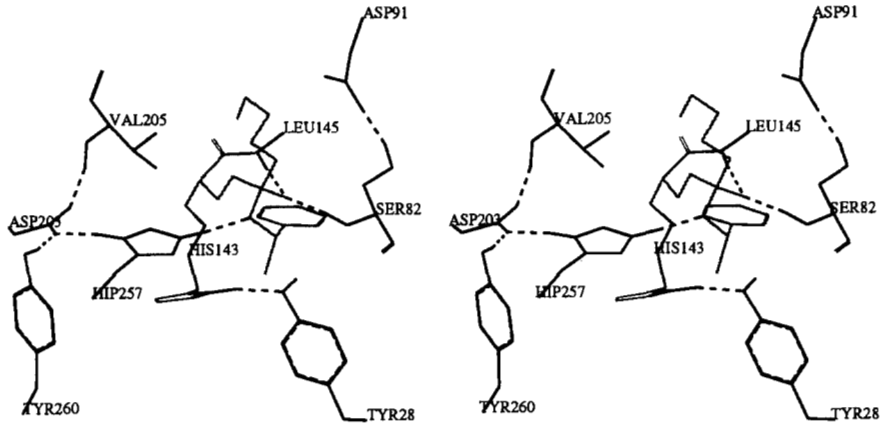

Fig. 7. Hydrogen bonds and polar interactions in the active site of the R-PHERM structure. Hydrogen bonds are shown with dashed lines and the serine–substrate transition-state complex with gray lines.

and vice versa. In addition, we used carbonyl oxygen probes to identify binding sites for the polar groups of the leaving diacyl glyceride part of the substrate.

The calculated properties of the binding sites of the *R. miehei* and the *H. lanuginosa* lipases were similar. This is not surprising because the active sites of these 2 lipases are known to be similar. The overall amino acid sequence homology between these lipases is around 30%, with higher homologies in the active sites. The main-chain folds of the active sites are almost identical. General descriptions of the structures of the *H. lanuginosa* and related lipases have recently been published (Derewenda et al., 1994). The similar binding properties predicted by our calculations indicate that the methods used are robust with respect to perturbations of the starting models.

The fact that no binding sites for a leaving diacyl glyceride could be traced by the GRID calculations can be explained by considering how the lipase would use the substrate-binding energy to maximize the catalytic efficiency. If the leaving group would bind strongly to the active site, the enzyme would suffer product inhibition. The specific binding site for the aliphatic chain, which forms the acyl enzyme complex, may be important for directing the substrate into the right binding mode for catalysis. The GRID calculations indicated that the active sites of the lipases investigated are amphiphilic. The active sites have channel-like hydrophilic sites separated from the amphiphilic sites. This hydrophilic site may be used by the enzymes to direct water molecules from the water phase to the reaction center. Water hydrolyzes the acyl enzyme. GRID calculations of an acyl enzyme intermediate suggested that the hydrophilic site ends up in a favorable position for a nucleophilic attack on the reactive carbonyl carbon atom of the acyl enzyme. The activity of water may be reduced in the hydrophobic interface in which the lipases act. Thus, high-affinity sites for water can be important to provide a sufficient water activity in the active site.

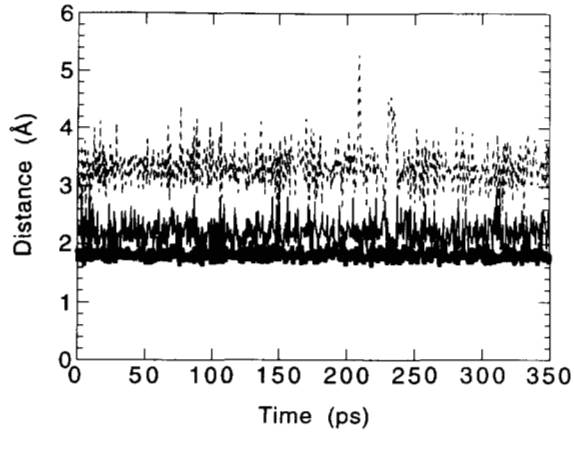

Fig. 8. Distances from the oxyanion of the transition state to its interaction partners during the prolonged simulation of the R-PHERM structure. The distance to the hydrogen atoms of the backbone amides of Ser-82 and Leu-145 are shown with a thick and a thin line, respectively. The distance to the hydrogen atom of the hydroxyl group of Tyr-28 is shown with a dashed line.

GRID calculations of the *C. rugosa* lipase indicated an aliphatic site and a hydrophilic site whose stereochemical positions in relation to the α/β-hydrolase fold (Ollis et al., 1992) were similar to the corresponding steric conditions in the *R. miehei* and *H. lanuginosa* lipases. In the *C. rugosa* lipase, the aliphatic site is positioned in a long tunnel inside the protein. The tunnel was recently observed in X-ray crystallography studies (Grochulski et al., 1994b) and has now been shown to be involved in the binding of the scissile fatty acid chain (Grochulski et al., 1994a).

The aspartic acid residues of the catalytic triads are buried in the enzymes, which may cause a large increase in their pK_a values. Experimental studies of the catalytic triad in serine proteases indicate that the buried aspartate residue in the triad has a pK_a value lower than 1 (Porubcan et al., 1979; Bachovchin et al., 1981; Kossiakoff & Spencer, 1981). The carboxyl group of the aspartate in the catalytic triads of the lipases investigated was strongly hydrogen bonded in the molecular dynamics simulations. The hydrogen bonds stabilize the negative charge of the ionized carboxyl groups. Therefore, they may be important in establishing low pK_a values of these aspartate residues.

The stereochemistry of the oxyanion hole of the lipases investigated has not yet been defined unambiguously. The backbone amide and the side chain of Ser-82 in the *R. miehei* lipase have been proposed to contribute to the oxyanion hole (Brzozowski et al., 1991). However, as declared by Derewenda and Sharp (1993), the resolutions of the X-ray crystal structures are not sufficient for giving a clear picture of the exact stereochemistry of the oxyanion hole in the *R. miehei* lipase. From our calculations, we suggest that the backbone amides of Leu-145 and Ser-82 contribute to the oxyanion hole. Site-directed mutagenesis studies of a homologous lipase (Beer et al., 1993) from *Rhizopus niveus*

showed that the turnover of the lipases was largely reduced when a threonine, in an analogous position to that of Ser-82 in the *R. miehei* lipase, was replaced by an alanine residue. Because Ser-82 belongs to a flexible lid, we speculate that the role of the side chain of Ser-82 is to anchor the backbone in a position favorable for an oxyanion hole. The side chain of Ser-82 of the *R. miehei* lipase formed a stable hydrogen bond to the side chain of Asp-91 in our molecular dynamics simulations. From molecular dynamics simulations of the *R. miehei* lipase, we suggest that the hydroxyl group of Tyr-28 may contribute to the stabilization of the oxyanion. In the X-ray crystal structure of the *R. miehei* lipase complexed with a transition-state inhibitor, the distance between the hydroxyl group of the tyrosine residue and the phosphonyl oxygen atom is longer than a well-developed hydrogen bond. However, rearrangements that were observed in some of our free energy calculations caused the tyrosine residue to form a favorable interaction with the oxyanion. No enzymatic reaction could be detected when this tyrosine residue was replaced by phenylalanine in the lipase from *R. niveus* by site-directed mutagenesis (Beer et al., 1993). However, these as well as previous ideas about the structure of the oxyanion hole are still speculative. High-resolution X-ray crystallographic and NMR studies of lipase–inhibitor complexes may shed further light on this important property of the enzyme.

Lipases from *R. miehei* and *H. lanuginosa* are excellent catalysts for racemic resolutions of many secondary alcohols. It is, therefore, of interest to study the molecular origins of the enantioselectivities of the reactions of these alcohols. Molecular dynamics simulations and energy minimizations of transition-state models of chiral ester substrates in the active sites of the *R. miehei* and *H. lanuginosa* lipases suggested that the binding orientations of the substrates are different for the enantiomers of the 1-phenylethyl and the 2-octyl hexanoate substrates. The substrates investigated had 1 methyl group and 1 phenyl or hexyl group attached to the chiral carbon atom. In our calculations, the large groups, phenyl or hexyl, bonded similarly in both lipases. However, the large groups of the enantiomers occupied different sites in the enzymes. A binding site that favorably accommodated the methyl group of the *R*-enantiomers was not accessible for the methyl groups of the slow-reacting *S*-enantiomers.

Recent X-ray crystallography studies of the *C. rugosa* lipase complexed with transition-state analogues for the hydrolysis of enantiomers of methyl esters showed that the analogue for the slow-reacting enantiomer had lost the hydrogen bond between the catalytic histidine residue and the oxygen atom of the leaving methyl group (Cygler et al., 1994). This orientation of the inhibitor is inconsistent with the reaction mechanism of the lipases. Molecular mechanics calculations showed that a reorientation of the slow-reacting methyl ester, in which the oxygen of the methyl group was moved into hydrogen bonding distance to the catalytic histidine, caused strain in the molecule. In our study of the 2 fungal lipases, the models of the transition states of the slow-reacting enantiomers retained the hydrogen bonding network consistent with the reaction mechanism, but they were more strained than the corresponding transition states of fast-reacting enantiomers. The main reason for this strain is that the large groups of transition states of the slow-reacting *S*-enantiomers were interacting unfavorably with the enzyme. The only way to reorient these large groups to interact favorably and still retain the necessary hydrogen bonding network is to force the small group, attached to the chiral carbon, into a very unfavorable position where it bumps into the backbone of the enzyme very close to the oxyanion hole. Actually, this was the case in some of the starting structures of the transition states of the slow-reacting *S*-enantiomers. Because lipases and esterases share a common α/β-hydrolase fold (Ollis et al., 1992) around the reaction centers, it is likely that the overall stereochemistry of the catalytic machinery's are similar. Therefore, the observations in this study may be common among many enzymes within this family.

Free energy difference calculations of the enantiomeric transition states, using a thermodynamic integration method, failed due to statistical and systematic errors in the calculations. One reason for this might be that the simulation times were too short for sufficient equilibrations of the molecular systems. The observed large movements of the phenyl and hexyl groups attached to the chiral carbon atom of the substrates may require long simulation times. In the light of recent studies by Pearlman (1994), in which time scales of more than 1 ns were needed to calculate solvation energies of 2 neon atoms, it is not surprising that our calculations were impaired by large errors. Our results do not disqualify the free energy methods but indicate that these methods are not as straightforward as sometimes indicated in the literature. Further calculations using longer simulation times and larger computer resources are needed to derive quantitative values of the free energies.

The molecular dynamics simulations were performed in vacuum to save computer time. This is a poor model of the environment of a protein solvated by water. The main effect of water is the screening of the electrostatic interactions. In our case, we modeled a lipase acting at a hydrophobic interface. One can assume that the electrostatic screening is much weaker at such an interface than in water. In a study parallel to this one (Norin et al., 1994), we made molecular dynamics simulations of the closed *R. miehei* lipase in water, in vacuum, and in methyl hexanoate. These studies showed that the electrostatic interactions of the protein were similar in vacuum and in methyl hexanoate.

Materials and methods

Molecular modeling equipment

All calculations were performed on an Evans and Sutherland ESV33/LCS workstation. Manipulations of molecules, graphic evaluations of GRID calculations, energy minimizations, and molecular dynamics simulations were done using the molecular modeling program SYBYL version 6.03 (Tripos Associates, 1993).

Lipase structures

Two X-ray crystal structures (U. Derewenda et al., 1992) of enzyme–inhibitor complexes were used as a models for the *R. miehei* lipase. Lipase from *C. rugosa* was modeled from a crystal structure determined by Grochulski et al. (1993). These structures have entry numbers 4TGL, 5TGL, and 1CRL, respectively, in the Brookhaven Protein Data Bank (Bernstein et al., 1977; Abola et al., 1987). The structure of the *H. lanuginosa* lipase was taken from an X-ray crystal structure, resolved at 2 Å, of an enzyme–inhibitor complex kindly provided by NOVO/Nordisk A/S, Bagsvaerd, Denmark, with permission from the crystallographers at the University of York.

GRID calculations

Version 10 of the GRID program (Goodford, 1985) was used to map the active sites of lipases from *R. miehei*, *H. lanuginosa*, and *C. rugosa*. This version of the program makes use of recent developments of the GRID force field (Boobbyer et al., 1989; Wade et al., 1993; Wade & Goodford, 1993). The computational procedures of the GRID method are well described by Goodford (1985). The inhibitors and all water molecules were removed from the structures. Models of acyl enzyme intermediates were constructed by joining a hexanoate group with the Oγ atom of the active serine residue of the lipases. The stereochemistry of the carbonyl group was adjusted by superimposing the carbonyl carbon and oxygen atoms upon the phosphonyl group of the inhibitor in the X-ray crystal structure. The aliphatic carbon atoms of the hexanoate group were placed in favorable binding regions calculated by the GRID program. The structures of the active serine residue and of the acyl group were then further refined by energy minimization using the AMBER force field (Weiner et al., 1984). GRID force field parameters for the acyl group were taken from similar atoms in the GRID force field. All structures were processed by the GRIN module of the GRID program to prepare input files for the GRID calculations. The GRID calculations were performed using standard probes supplied by the program. The calculations modeled the lipases when acting at a hydrophobic interface or in an organic solvent. Therefore, we used a dielectric constant of 4 instead of 80 for the environment of the lipases. The LEAU = 2 option in the GRID program was used to model water bridges between the water probe and the protein. Active sites of the lipases were centered in a box of the dimensions 20 × 20 × 30 Å. Interactions between the probe and the protein were calculated at grid points, 0.5 Å apart.

Computational procedures in energy minimizations and molecular dynamics simulations

This section describes the procedures for calculations of the *R. miehei* lipase. The structure of the *H. lanuginosa* lipase is similar to that of the lipase from *R. miehei*. The *H. lanuginosa* lipase was superimposed on the *R. miehei* lipase structure. The amino acids of the *H. lanuginosa* lipase were treated in the same way as their structural homologues in the *R. miehei* lipase. The computational procedures were the same for both lipases. Only the amino acid residues within 8 Å from any atom of the inhibitor in the X-ray crystal structure of the *R. miehei* lipase were allowed to move. Between 8 and 12 Å, only the side chains were allowed to move and the remaining parts of the lipases were constrained at the starting structures. All water molecules were removed from the calculations. In all energy calculations a distance-dependent dielectric constant ($\epsilon = r$) was used. Hydrogen positions were calculated by the BIOPOLYMER module of SYBYL. The all-atom AMBER force field (Weiner et al., 1986) was applied to amino acid residues within 6 Å from the inhibitor. Other residues were treated by the united atom AMBER force field (Weiner et al., 1984). The force field parameters that were added are shown in Table 3. Partial charges of the atoms at the transition states were calculated by a semi-empirical method (Besler et al., 1990) using the MOPAC 6.0 ESP program. A more detailed description of the procedure is given in a previous paper (Norin et al., 1993). Nonbonded interactions were truncated at 10 Å.

Table 3. *Nonstandard force field parameters used in the calculations*

AMBER atoms	Equilibrium angle (deg)	Bending constant (kcal mol^{-1} deg^{-2})
CA-CT-OS	109.5	50
OH-CT-OS	109.5	50

Energy minimizations were performed by means of the Powell minimizer in SYBYL. All structures were subjected to 200 steps of energy minimization before the molecular dynamics simulations. These simulations were performed with constraints on all bond lengths using the SHAKE algorithm (Ryckaert et al., 1977). A time step of 2 fs was used. All simulations were equilibrated by raising the temperature to 300 K during 1.2 ps, followed by a simulation of 10 ps at 300 K.

Preparation of starting models of enzyme–substrate transition-state complexes

The transition-state model and the substrates are shown in Figure 1. Tetrahedral covalent complexes, in which the Oγ atom of the active serine residue is connected to the carbonyl carbon atom of the substrates, were built using SYBYL. The phosphonyl groups in the X-ray crystal structures of the transition-state inhibitor complexes were used to adjust torsional angles to prepare a plausible stereochemistry of the reaction center. GRID calculations guided us in adjusting the positions of the alkyl and the aromatic groups of the substrates. The aliphatic chains of the acyl moiety of the substrates were placed in an aliphatic site calculated by GRID (see Results). The leaving alkoxyl group was placed in a site opposite to the aliphatic site. GRID calculations were used to visualize unfavorable contacts between the substrate and the enzyme. In analogy with serine proteases, a protonated histidine residue in the catalytic triad was assumed to be present at the transition state.

Calculation of energy minima of the enzyme–substrate complexes

The energies and structures of the substrate–enzyme complexes were calculated by a combined energy minimization and molecular dynamics protocol that we had used previously in calculations of substrate–chymotrypsin complexes (Norin et al., 1993). Energy minima of the substrate–lipase complexes were found by molecular dynamics simulations in vacuum, in which the molecules were repeatedly heated to 300 K and slowly cooled to 1 K. After an initial equilibration, the temperature of the molecular system was decreased during 1.5 ps to 1 K. Then the temperature was raised during 1.2 ps to 300 K, followed by equilibration during 6 ps before the next cooling period. Ten cycles of heating and cooling were run. The total simulation time was 98 ps. The conformations trapped at 1 K were subjected to 500 steps of energy minimization.

Free energy calculations

The free energy differences between the enantiomers of the substrate–enzyme transition-state complexes were calculated by

means of thermodynamic integration. The method used here is similar to the calculations of differences between the free energies of binding of stereoisomers to thermolysin, reported by Edholm and Ghosh (1993). The chiral carbon atoms of the leaving substrate alcohol groups were transformed between the 2 enantiomeric states by applying a perturbing potential to an improper dihedral angle. The improper dihedral, χ, was defined as the angle between a bond joining the chiral carbon atom with the neighboring oxygen atom and the plane containing the chiral carbon atom and neighboring carbon atoms. The perturbing potential was dependent on a parameter λ, which changed from 0 to 1 between the initial and final states of the calculation. The perturbing potential was described by the following equation:

$$V(\chi,\lambda) = \tfrac{1}{2}C\{[\chi_i - \chi_0 - \lambda(\chi_1 - \chi_0)]^2\}, \quad (1)$$

where χ_i is the current improper dihedral and C is a constant set at 0.02 kcal mol^{-1} deg^{-2}. The equilibrium improper torsional angle was changed by setting χ_0 and χ_1 at $-36°$ and $+36°$, respectively. The difference $G(\lambda = 1) - G(\lambda = 0)$ can be calculated by a thermodynamic integration formula:

$$\Delta G \approx \sum_{\lambda=0}^{\lambda=1} \left\langle \frac{\partial V(\lambda)}{\partial \lambda} \right\rangle_{\lambda_i} \Delta\lambda. \quad (2)$$

The bracket denotes averages sampled from molecular dynamics simulations at subsequent values of λ. The step size, $\Delta\lambda$, is the difference of the λ values of 2 molecular dynamics simulations. Molecular dynamics simulations at each value of λ were performed by raising the temperature during 1.2 ps to 300 K, followed by equilibration during 2.4 ps. Data for calculation of the average potential derivative were collected from each step in the simulation during the following 2.4 ps. Before each molecular dynamics simulation, the molecules were energy minimized using 200 steps of energy minimization. Before the free energy calculations, the structures were equilibrated during 10 ps using the starting conditions of the restraining potential. The hydrogen atom that is bonded to the chiral carbon atom would be forced into highly strained bonding angles around the chiral carbon atom. This problem was circumvented by removing all apolar hydrogen atoms and applying the united atom force field to the entire system. The molecular dynamics simulations were otherwise performed as described above.

Acknowledgments

We thank the crystallographic group at the University of York and Alan Svendsen and Ole Olsen at NOVO/Nordisk A/S, Bagsvaerd, Denmark, for providing the crystal structures of the lipases and for valuable discussions. Financial support from the Swedish Research Council for Engineering Science (TFR), the Swedish Natural Science Research Council (NFR), and the Swedish Board for Technical Development (NUTEK) are gratefully acknowledged. We also thank Olle Edholm at the Department of Theoretical Physics, KTH, and Gunhild Aulin-Erdtman for valuable discussions.

References

Abola EE, Bernstein FC, Bryant SH, Koetzle TF, Weng J. 1987. Protein Data Bank. In: Allen FH, Bergerhoff G, Sievers R, eds. *Crystallographic databases—Information content, software systems, scientific applications*. Bonn/Cambridge/Chester: Data Commission of the International Union of Crystallography. pp 107–132.

Bachovchin WW, Kaiser R, Richards JH, Roberts JD. 1981. Catalytic mechanism of serine proteases: Reexamination of the pH dependence of the histidyl 1J13C2-H coupling constant in the catalytic triad of α-lytic protease. *Proc Natl Acad Sci USA 78*:7323–7326.

Beer HD, Wohlfahrt G, McCarthy JEG, Menge U, Schomburgh D, Schmid RD. 1993. Computer-aided site-directed mutagenesis: A tool in the investigation of the molecular mechanism of lipase catalysis. Poster presentation at "Lipases: Structure function and protein engineering," Elsinore, Denmark.

Bernstein FC, Koetzle TF, Williams GJB, Meyer EF Jr, Brice MD, Rodgers JR, Kennard O, Shimanouchi T, Tasumi M. 1977. The Protein Data Bank: A computer-based archival file for macromolecular structures. *J Mol Biol 112*:535–542.

Besler BH, Merz KM Jr, Kollman PA. 1990. Atomic charges derived from semiempirical methods. *J Comput Chem 11*:431–439.

Boobbyer DNA, Goodford PJ, McWhinnie PM, Wade RC. 1989. New hydrogen-bond potentials for use in determining energetically favorable binding sites on molecules of known structure. *J Med Chem 32*:1083–1094.

Brady L, Brzozowski AM, Derewenda ZS, Dodson E, Dodson G, Tolley S, Turkenburg JP, Christiansen L, Huge-Jensen B, Norskov L, Thim L, Menge U. 1990. A serine protease triad forms the catalytic centre of a triacylglycerol lipase. *Nature 343*:767–770.

Brzozowski AM, Derewenda U, Derewenda ZS, Dodson GG, Lawson DM, Turkenburg J, Bjorkling F, Huge-Jensen B, Patkar SA, Thim L. 1991. A model for interfacial activation in lipases from the structure of a fungal lipase-inhibitor complex. *Nature 351*:491–494.

Byberg JR, Jørgensen FS, Hansen S, Hough E. 1992. Substrate-enzyme interactions and catalytic mechanism in phospholipase C: A molecular modeling study using the GRID program. *Proteins Struct Funct Genet 12*:331–338.

Cygler M, Grochulski P, Kazlauskas RJ, Schrag JD, Bouthillier F, Rubin B, Serreqi AN, Gupta AJ. 1994. A structural basis for the chiral preferences of lipases. *J Am Chem Soc 116*:3180–3186.

Derewenda U, Brzozowski AM, Lawson DM, Derewenda ZS. 1992. Catalysis at the interface: The anatomy of a conformational change in a triglyceride lipase. *Biochemistry 31*:1532–1541.

Derewenda U, Swenson L, Green R, Wei Y, Dodson GG, Yamaguchi S, Haas MJ, Derewenda ZS. 1994. An unusual buried polar cluster in a family of fungal lipases. *Nature Struct Biol 1*:36–47.

Derewenda ZS, Derewenda U, Dodson GG. 1992. The crystal and molecular structure of the *Rhizomucor miehei* triacylglyceride lipase at 1.9 Å resolution. *J Mol Biol 227*:818–839.

Derewenda ZS, Sharp AM. 1993. News from the interface: The molecular structures of triacylglyceride lipases. *Trends Biochem Sci 18*:20–25.

Edholm O, Ghosh I. 1993. Hysteresis and statistical errors in the free energy perturbation L to D amino acid conversion. *Mol Sim 10*:241–253.

Goodford PJ. 1985. A computational procedure for determining energetically favorable binding sites on biologically important macromolecules. *J Med Chem 28*:849–857.

Grochulski P, Bouthillier F, Kazlauskas RJ, Serreqi AN, Schrag JD, Ziomek E, Cygler M. 1994a. Analogs of reaction intermediates identify a unique substrate binding site in *Candida rugosa* lipase. *Biochemistry 33*:3494–3500.

Grochulski P, Li Y, Schrag JD, Bouthillier F, Smith P, Harrison D, Rubin B, Cygler M. 1993. Insights into interfacial activation from an open structure of *Candida rugosa* lipase. *J Biol Chem 268*:12843–12847.

Grochulski P, Li Y, Schrag JD, Cygler M. 1994b. Two conformational states of *Candida rugosa* lipase. *Protein Sci 3*:82–91.

Janssen AJM, Klunder AJH, Zwanenburg B. 1991. Resolution of secondary alcohols by enzyme-catalyzed transesterification in alkyl carboxylates as the solvent. *Tetrahedron 47*:7645–7662.

Kossiakoff AA, Spencer SA. 1981. Direct determination of the protonation states of aspartic acid-102 and histidine-57 in the tetrahedral intermediate of the serine proteases: Neutron structure of trypsin. *Biochemistry 20*:6462–6474.

Macfarlane ELA, Roberts SM, Turner NJ. 1990. Enzyme-catalysed interesterification procedure for the preparation of esters of a chiral secondary alcohol in high enantiomeric purity. *J Chem Soc Chem Commun 7*:569–571.

Norin M, Haeffner F, Hult K, Edholm O. 1994. Molecular dynamics simulations of an enzyme surrounded by vacuum, water or a hydrophobic solvent. *Biophys J 67*:548–559.

Norin M, Hult K, Mattson A, Norin T. 1993. Molecular modelling of chymotrypsin-substrate interactions: Calculation of enantioselectivity. *Biocatalysis 7*:131–147.

Ollis DL, Cheah E, Cygler M, Dijkstra B, Frolow F, Franken SM, Harel M,

Remington SJ, Silman I, Schrag J, Sussman JL, Verschueren KHG, Goldman A. 1992. The α/β hydrolase fold. *Protein Eng 5*:197–211.

Pearlman DA. 1994. Free energy derivatives: A new method for probing the convergence problem in free energy calculations. *J Comput Chem 15*:105–123.

Porubcan MA, Westler WM, Ibañez IB, Markley JL. 1979. (Diisopropylphosphoryl)serine proteinases. Proton and phosphorus-31 nuclear magnetic resonance-pH titration studies. *Biochemistry 18*:4108–4116.

Ryckaert JP, Ciccotti G, Berendsen HJC. 1977. Numerical integration of the cartesian equations of motion of a system with constraints: Molecular dynamics of *n*-alkanes. *J Comput Phys 23*:327–341.

Sarda L, Desnuelle P. 1958. Action de la lipase pancréatique sur les esters en émulsion. *Biochim Biophys Acta 30*:513–521.

Schrag JD, Cygler M. 1993. 1.8 Å refined structure of the lipase from *Geotrichum candidum*. *J Mol Biol 230*:575–591.

Sonnet PE. 1987. Kinetic resolutions of aliphatic alcohols with a fungal lipase from *Mucor miehei*. *J Org Chem 52*:3447–3479.

Sonnet PE, Baillargeon MW. 1987. Kinetic resolution of secondary alcohols with commercial lipases. *J Chem Ecol 13*:1279–1292.

Sonnet PE, Moore G. 1988. Esterification of 1- and *rac*-2-octanols with selected acids and acid derivatives using lipases. *Lipids 23*:955–960.

Tripos Associates. 1993. *Molecular modelling program SYBYL 6.03*. St. Louis, Missouri: Tripos Associates.

van Tilbeurgh H, Egloff MP, Martinez C, Rugani N, Verger R, Cambillau C. 1993. Interfacial activation of the lipase–procolipase complex by mixed micelles revealed by X-ray crystallography. *Nature 362*:814–820.

van Tilbeurgh H, Sarda L, Verger R, Cambillau C. 1992. Structure of the pancreatic lipase–procolipase complex. *Nature 359*:159–162.

von Itzstein M, Wu WY, Kok GB, Pegg MS, Dyason JC, Jin B, Van Phan T, Smythe ML, White HF, Oliver SW, Colman PM, Varghese JN, Ryan DM, Woods JM, Bethell RC, Hotham VJ, Cameron JM, Penn CR. 1993. Rational design of potent sialidase-based inhibitors of influenza virus replication. *Nature 363*:418–423.

Wade RC, Clark KJ, Goodford PJ. 1993. Further development of hydrogen bond functions for use in determining energetically favorable binding sites on molecules of known structure. 1. Ligand probe groups with the ability to form two hydrogen bonds. *J Med Chem 36*:140–147.

Wade RC, Goodford PJ. 1993. Further development of hydrogen bond functions for use in determining energetically favorable binding sites on molecules of known structure. 2. Ligand probe groups with the ability to form more than two hydrogen bonds. *J Med Chem 36*:148–156.

Weiner SJ, Kollman PA, Case DA, Singh UC, Ghio C, Alagona G, Profeta S Jr, Weiner P. 1984. A new force field for molecular mechanical simulation of nucleic acids and proteins. *J Am Chem Soc 106*:765–784.

Weiner SJ, Kollman PA, Nguyen DT, Case DA. 1986. An all atom force field for simulations of proteins and nucleic acids. *J Comput Chem 7*:230–252.

Winkler FK, D'Arcy A, Hunziker W. 1990. Structure of human pancreatic lipase. *Nature 343*:771–774.